Fuel 279 (2020) 118302

Contents lists available at ScienceDirect

Fuel

journal homepage: www.elsevier.com/locate/fuel

Full Length Article

Effect of superficial velocity on liquid injectivity in SAG foam EOR. Part 2: Modelling

Jiakun Gong[a,*], Wendy Flores Martinez[a], Sebastien Vincent-Bonnieu[a,b], Ridhwan Zhafri Kamarul Bahrim[c], Che A Nasser Bakri Che Mamat[c], Raj Deo Tewari[c], Mohammad Iqbal Mahamad Amir[c], Rouhollah Farajzadeh[a,b], William Rossen[a]

[a] Department of Geoscience and Engineering, Delft University of Technology, 2628 CN Delft, The Netherlands
[b] Shell Global Solutions International B.V., 1031 HW Amsterdam, The Netherlands
[c] PETRONAS, Kuala Lumpur 50088, Malaysia

ARTICLE INFO

Keywords:
Foam
Enhanced oil recovery
Surfactant-alternating-gas
Injectivity
Superficial velocity
Bank-propagation model

ABSTRACT

Surfactant-alternating-gas (SAG) is a favored method of foam injection, which has been proved as an efficient way for enhancing oil recovery. However, foam flow is extremely complicated, and there are still unsolved problems for foam application. One is liquid injectivity. Our previous studies suggest that the injectivity in a SAG process is determined by propagation of several banks near the injection well that are not represented by current foam models. Uniform bank properties were assumed. However, in a companion paper, our experimental results show that the dimensionless propagation velocity and the total mobility of banks during the liquid-injection period depends on superficial velocity. Shearing-thinning behavior is observed. In radial flow, the superficial velocity varies with distance from the well. In this study, we scale-up the experimental results using a radial bank-propagation model. The comparison of liquid injectivity estimated from conventional foam simulators (Peaceman equation) and the bank-propagation model show that the conventional foam models cannot represent the effect of the superficial-velocity-dependent fluid properties during liquid injection in a SAG process. The shear-thinning behavior can lead to much better liquid injectivity than expected, which should be accounted for in a field application of a SAG foam process.

1. Introduction

Gas injection is one of the most common methods for enhancing oil recovery. It can often ultimately recover all the oil where it sweeps. However, it often suffers from poor sweep efficiency, mainly caused by reservoir heterogeneity, viscous instability and gravity override [1]. Foam can address all these three issues [2–4].

Foam is placed into reservoirs primarily in two ways: one is co-injecting gas and surfactant solution, the other is injecting gas and liquid slugs alternatively [2,4–9], so-called surfactant-alternating-gas, or SAG. There are also other methods for foam injection, such as dissolving surfactant into supercritical CO_2 [10,11]. Among these methods, SAG is a favored one [8]. Previous studies showed that injectivity of gas is excellent. The gas injection rate should be adjusted in order to maintain the maximum injection pressure allowed without fracturing the injection well [8]. However, the advantage of good gas injectivity is reduced massively by the poor liquid injectivity in a SAG process [12,13].

Liquid injectivity directly following foam is very poor, as discussed in the literature [14–19]. Most of these studies were focused on acid diversion, in which poor liquid injectivity is the goal. In our previous studies [14,20], instead of examining liquid injectivity following co-injection of surfactant solution and gas, we studied liquid injectivity following gas in a SAG process. We found that a collapsed-foam region forms near the inlet during the gas-injection period and slowly propagates downstream. This collapsed-foam region has major impact on the subsequent liquid injectivity. Various banks are observed during the gas- and liquid-injection periods. During the gas-injection period, the core is occupied by the collapsed-foam bank and the weakened-foam bank. During the liquid-injection period, the collapsed-foam bank, forced-imbibition bank and gas-dissolution bank are observed [14]. These banks are not described by current foam models.

We then proposed a simplified bank-propagation model based on our experimental findings [20]. The liquid injectivity estimated by conventional foam simulators based on the Peaceman equation and the bank-propagation model were compared. Results show that the

* Corresponding author.
E-mail address: j.gong@tudelft.nl (J. Gong).

https://doi.org/10.1016/j.fuel.2020.118302
Received 13 October 2019; Received in revised form 30 May 2020; Accepted 2 June 2020

Nomenclature

A	power-law parameter, $(m^2/(Pa\ s)\ (ft/day)^{-B}$ (Eq. (5))
B, D, F, H	power-law parameter, dimensionless (Eqs. (5)–(8))
C	power-law parameter, $(ft/day)^{-D}$ (Eq. (6))
E	power-law parameter, $(m^2/(Pa\ s)\ (ft/day)^{-F}$ (Eq. (7))
G	power-law parameter, $(ft/day)^{-H}$ (Eq. (8))
GPV	grid-block pore volume, dimensionless
h	reservoir height, m
l, l_1, l_2	linear position, m
L	grid-block size, m
LPV	local pore volume, dimensionless; based on pore volume from given location back to injection face
Δp_b	pressure difference across each bank for linear-flow and radial-flow models, Pa
Δp_F	pressure difference across the foam bank for linear-flow and radial-flow models, Pa
Δp_{FCG}	pressure difference across the collapsed-foam bank during gas injection for linear-flow and radial-flow models, Pa
Δp_{FCL}	pressure difference across the collapsed-foam bank during liquid injection for linear-flow and radial-flow models, Pa
Δp_{FI}	pressure difference across the forced-imbibition bank during liquid injection for linear-flow and radial-flow models, Pa
Δp_{GD}	pressure difference across the gas-dissolution bank during liquid injection for linear-flow and radial-flow models, Pa
Δp_t	total pressure difference for linear-flow and radial-flow models, Pa
PV	pore volumes, dimensionless (based on the total pore volume of a core or a formation)
Q_0	reference volumetric injection rate, m^3/s
Q_t	total volumetric flow rate, m^3/s
r, r_1, r_2	radial position, m
r_e	outer radius for Peaceman equation, m
r_w	wellbore radius, m
SAG	surfactant-alternating-gas
S	cross-section area, m^2
S_w	water saturation, dimensionless
u_t	total superficial velocity, m/s
V_{GD}	dimensionless propagation velocity of the gas-dissolution bank at various radial positions, dimensionless
V_{FI}	dimensionless propagation velocity of the forced-imbibition bank at various radial positions, dimensionless
v_s	superficial velocity at various positions, m/s
λ_{tb}	total mobility of a bank, $m^2/Pa\ s$
λ_{tFI}	total mobility of the forced-imbibition bank, $m^2/Pa\ s$
λ_{tGD}	total mobility of the gas-dissolution bank, $m^2/Pa\ s$

conventional foam models do not represent the effect of gas injection on the subsequent liquid injectivity. They can greatly underestimate the liquid injectivity in a SAG process.

In our original model, the bank properties, i.e. the dimensionless propagation velocity and the total mobility, which served as inputs of the various banks, are assumed to be uniform within each bank. The total mobility ($\nabla p/u_t$) of a bank is determined from the pressure gradient (∇p) and the total superficial velocity (u_t) by applying Darcy's law (approximating foam flow as single-phase flow). The dimensionless propagation velocity of the front of a bank is determined from the position of the front; it is the volume injected divided by the cumulative pore volume from the position of the front back to the inlet. However, our recent experimental results [21] present that the forced-imbibition bank and gas-dissolution bank during liquid injection following gas show strong shear-thinning behavior. The properties of these two banks depend on the liquid superficial velocity. This suggests that in radial flow around the injection well, the dimensionless propagation velocity is not constant and the total mobility is not uniform within the forced-imbibition bank and the gas-dissolution bank. Modelling and upscaling a SAG foam process from laboratory scale is necessary for field-scale application. Although the simplified bank-propagation model involves many assumptions and approximations, it is the most direct way to scale-up our laboratory findings at this moment.

In this study, we incorporate the superficial-velocity-dependent bank properties into our bank-propagation model and, in turn, discuss the implications for field applications. We first fit a linear 1D model to coreflood data for both the gas-injection period and the liquid-injection period, which reflects propagation of various banks. We then assume the core-scale behavior can be scaled up to radial flow in field, and apply this bank-propagation model to the near-well region in a field application. In the end, we compare the results of our model to that of a foam simulator based on the conventional approach to represent foam

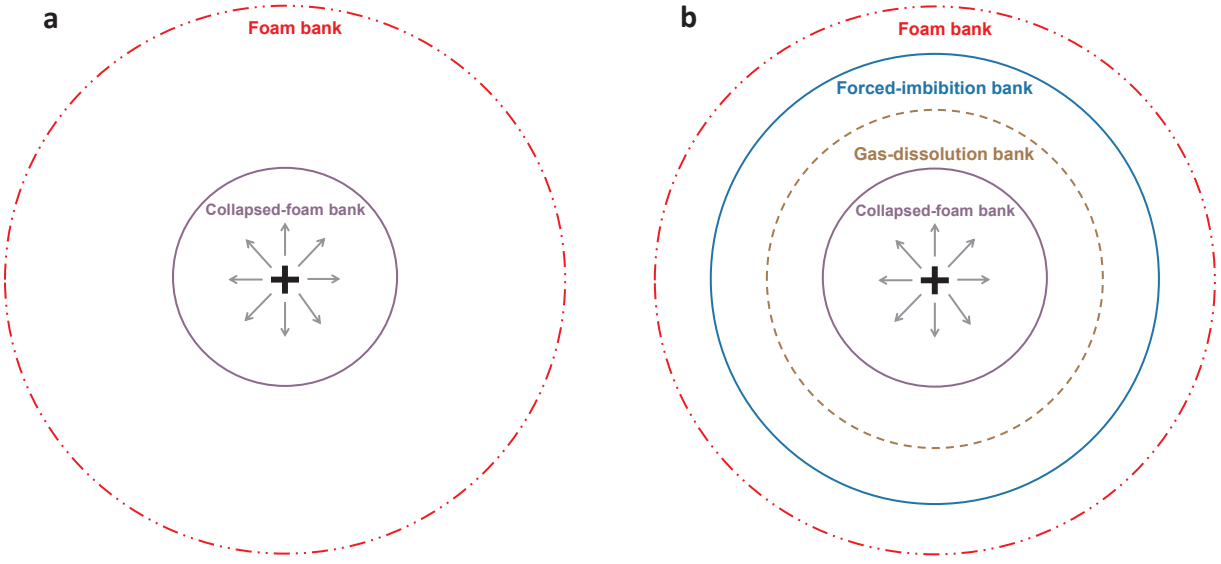

Fig. 1. Banks observed in SAG-foam coreflood experiments. (a) Banks during the gas-injection period. (b) Banks during the liquid-injection period.

and the Peaceman equation. We point out the potential errors in estimation of liquid injectivity given by the conventional foam simulator, and the importance of considering the shear-thinning behavior in estimating liquid injectivity in a SAG process.

2. Model description

The bank-propagation model is described in detail in our previous work [20]. Here we briefly introduce the model.

The bank-propagation model assumes that the core-scale behavior and the bank properties of the varies banks can be scaled up to field application. The total pressure difference is calculated by summing up the pressure differences across various banks that may appear during the gas-injection period and the liquid-injection period, respectively. Fig. 1 illustrates the banks in radial flow around an injection well.

The total pressure difference across a given section of a core during gas injection in a SAG process is the sum of the pressure differences across the foam bank Δp_F and the collapsed-foam bank Δp_{FCG} (as long as each bank is present in the given core section):

$$\Delta p_t = \Delta p_F + \Delta p_{FCG} \tag{1}$$

For the liquid-injection period, the total pressure difference is the sum of the pressure differences across the collapsed-foam bank Δp_{FCL}, the gas-dissolution bank Δp_{GD} and the forced-imbibition bank Δp_{FI}, as long as all are present:

$$\Delta p_t = \Delta p_{FCL} + \Delta p_{GD} + \Delta p_{FI} \tag{2}$$

The linear-flow model is used for fitting our results in coreflood experiments. For each bank b, Darcy's law for multi-phase flow is employed to calculate the pressure difference across that bank:

$$\Delta p_b = \int_{l_1}^{l_2} \frac{Q_t}{S\lambda_{tb}} dl = \frac{Q_t}{S}\frac{(l_2 - l_1)}{\lambda_{tb}} \tag{3}$$

where, in each bank, extending from positions l_1 to l_2, the total mobility (λ_{tb}) is assumed to be uniform in the original model [20]. If the given bank overlaps the entrance or the exit of the given core section, l_1 or l_2 represent the boundaries of the core section. Values of bank mobilities and dimensionless propagation velocities derived from our coreflood experiments are listed in our companion paper [21].

The radial-flow model applies the implications of our experimental findings to field application. Assuming uniform mobility for each bank b, Darcy's Law for radial multi-phase flow is employed to calculate the pressure difference across each bank:

$$\Delta p_b = \int_{r_1}^{r_2} \frac{Q_t}{2\pi r h \lambda_{tb}(r)} dr \tag{4}$$

where, in each bank, extending from r_1 to r_2, the total mobility ($\lambda_{tb}(r)$) is assumed to be uniform in the original model.

As mentioned above, uniform bank properties, i.e. the dimensionless propagation velocity and the total mobility, are assumed in our previous model. However, strongly shear-thinning behavior of the gas-dissolution bank and the forced-imbibition bank is observed in our recent coreflood experiments. The total mobilities and the propagation velocities of banks at various superficial velocities are derived from the pressure-gradient changes over time in the coreflood experiments [21]. By putting the data corresponding to various liquid superficial velocities together, we find that the propagation velocities and the total mobilities of the gas-dissolution bank and the forced-imbibition banks follow power-law relationships with the superficial velocities. The fit of the data to these equations is shown in the next section.

During liquid injection, for the gas-dissolution bank, the following formula applies:

$$\lambda_{tGD} = A v_s^{\ B} \tag{5}$$

$$V_{GD} = C v_s^{\ D} \tag{6}$$

For the forced-imbibition bank, the following formula applies:

$$\lambda_{tFI} = E v_s^{\ F} \tag{7}$$

$$V_{FI} = G v_s^{\ H} \tag{8}$$

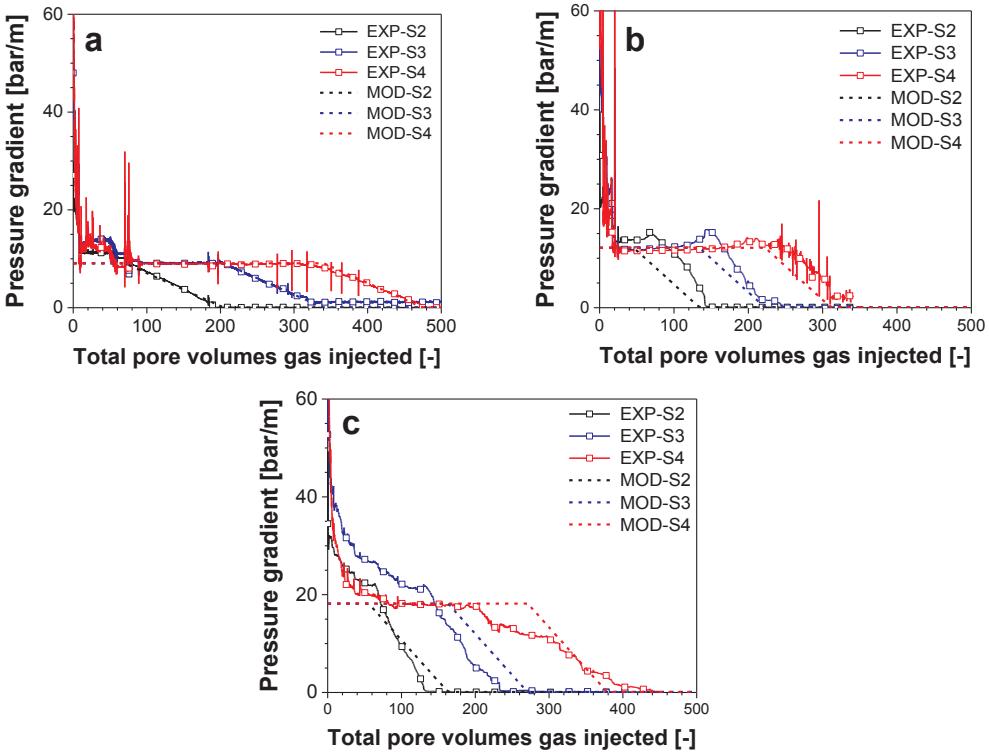

Fig. 2. Comparison of sectional pressure gradients in core-flood experiments with those obtained from the linear bank-propagation model, during gas injection following 0.95-quality foam at various superficial velocities. (a) 3 ft/day, (b) 6 ft/day, (c) 9 ft/day. EXP: experimental data. MOD: model fit. S2, S3, S4: Sections 2–4.

where λ_{tGD} and λ_{tFI} are the total mobilities of the gas-dissolution bank and the forced-imbibition bank, respectively; v_s is the superficial velocity at various radial positions, V_{GD} and V_{FI} are the dimensionless propagation velocities of the gas-dissolution bank and the forced-imbibition bank at various radial positions, respectively. *A-H* are power-law parameters.

The superficial velocity (v_s) at various radial positions is related to radial position (r) by

$$v_s = \frac{Q_t}{2\pi r h} \tag{9}$$

where r is the radial position, Q_t is the volumetric injection rate, h is the reservoir height.

We then modify the bank-propagation model proposed previously [14] in order to represent the effect of superficial velocity on liquid injectivity. For the gas-injection period, the bank properties are not significantly affected by the gas superficial velocity [21]. We therefore assume a uniform total mobility within each bank, and a constant dimensionless propagation velocity for the collapsed-foam bank. For the liquid-injection period, the bank properties of liquid flowing in the collapsed-foam bank is not significantly affected by the liquid superficial velocity. Uniform bank properties are assumed for this bank. For the gas-dissolution bank and the forced-imbibition bank, we assume power-law relations between mobilities, propagation velocites and position, as in Eqs. (5)–(9).

For the pressure gradients across the gas-dissolution bank and the forced-imbibition bank,

Eq. (4) becomes:

$$\Delta p_{GD} = \frac{\left(\frac{Q_t}{2\pi h}\right)^{1-B}}{AB}(r_2^B - r_1^B) \tag{10}$$

and

$$\Delta p_{FI} = \frac{\left(\frac{Q_t}{2\pi h}\right)^{1-F}}{EF}(r_2^F - r_1^F) \tag{11}$$

respectively.

3. Modelling results

3.1. Fit of linear model to coreflood experiments

As the first step, we compare the sectional pressure gradients estimated from our bank-propagation model with our experimental results. In the linear-flow model, we consider axial flow through a cylindrical core similar to the Berea core used in our experiments. The core is 17 cm long, with diameter 4 cm. The permeability is 160 mD, and the porosity is 0.2. The Berea core used in our experiments includes five sections; we focus on the three middle sections, each 4.2 cm long (Sections 2–4). In this way, the entrance and capillary-end are minimized.

As illustrated in Figs. 2 and 3, our bank-propagation model represents the core-scale behavior reasonably well, in terms of both mobilities and bank-propagation velocities.

For the gas-injection period, the bank-propagation model represents the propagation of the collapsed-foam bank well for the three superficial velocities examined (Fig. 2). In each case, a single dimensionless propagation velocity and total mobility gives a reasonable fit to the lab data of all the three sections. This indicates that the collapsed-foam bank propagates with a nearly constant velocity through the core. The bank-propagation model does not fit the experimental data at very early times. We do not attempt to represent the leading edge of the gas, and focus on the near-well behavior: propagation of the collapsed-foam bank and its effect on the subsequent liquid injectivity. More important, the initial state of the gas slug in these experiments (following full-strength foam) is not representative of that in the field in a SAG process, i.e. following a liquid slug [20].

For the liquid-injection period, we fit our bank-propagation model to the lab data for liquid injection at various superficial velocities, from 2 ft/day to 200 ft/day, following about 150 PV gas injection

(Fig. 3). After about 150 PV gas injection, the collapsed-foam bank penetrates into Section 2, but does not arrive at Sections 3 or 4. This

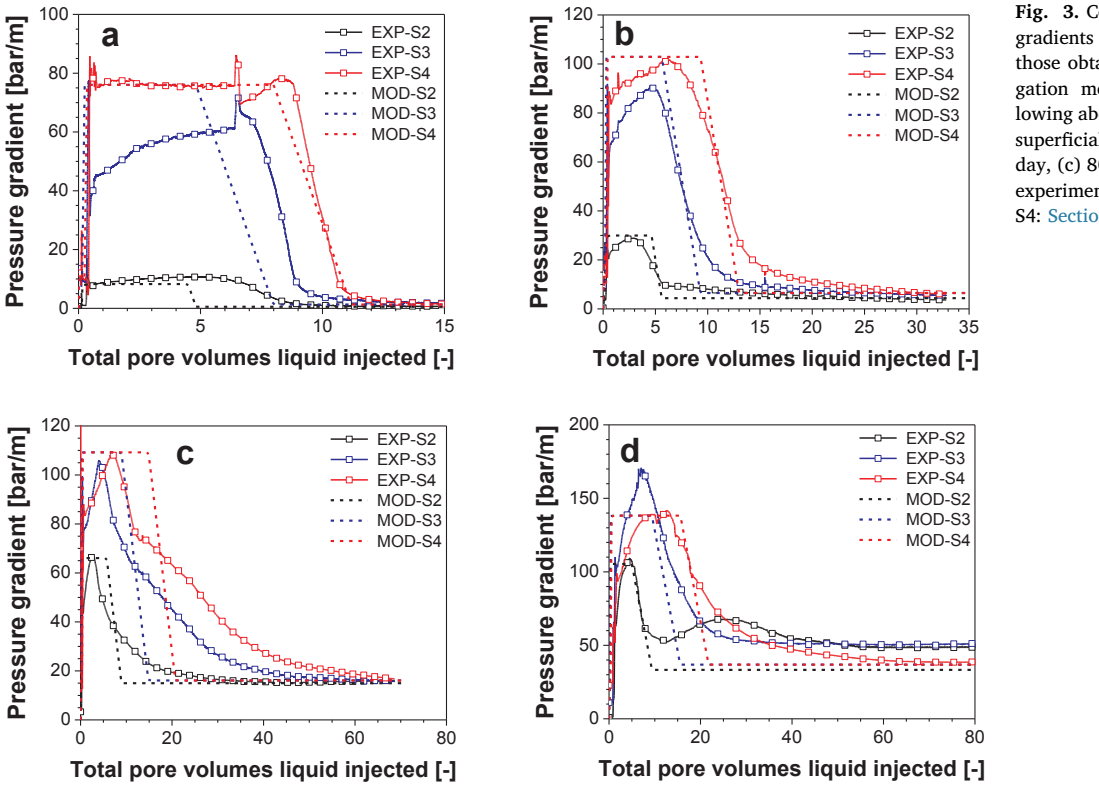

Fig. 3. Comparison of sectional pressure gradients in core-flood experiments with those obtained from the linear bank-propagation model during liquid injection following about 150 PV gas injection at various superficial velocities. (a) 2 ft/day, (b) 20 ft/day, (c) 80 ft/day, and (d) 200 ft/day. EXP: experimental data. MOD: model fit. S2, S3, S4: Sections 2–4.

explains why the pressure gradient in Section 2 is lower than that in the other two sections.

As presented in Fig. 3a and b, for relatively low superficial velocities, i.e. 2 ft/day and 20 ft/day, our bank-propagation model can fit the experimental data quite well. However, there is still some mismatch. For liquid injection at 2 ft/day, the gas-dissolution bank propagates more slowly in the bank-propagation model than in the coreflood experiment. In our model fit, we use the parameter values derived from the experimental data of Section 4 to fit all the sections. One other mismatch is the plateau value in pressure gradient for Section 3. In our model, the plateau value for Section 3 is the same as that for Section 4, while, in the lab data, it is lower than in Section 4, by about 15%. The main reason is that we assume a same permeability for all the three sections. However, the core is not completely homogeneous: the permeabilities for various sections are slightly different, i.e. about

170 mD for Section 3, and 150 mD for Section 4. The permeability ratio of Section 3 and 4 is about 1.13, which roughly represents the ratio of the plateau value in pressure gradient for Sections 3 and 4.

For large superficial velocities, i.e. 80 ft/day and 200 ft/day, our simple model represents the overall behavior, though it cannot capture all the details (Fig. 3c and d). The plateau in pressure gradient is not as obvious as in the cases for liquid injection at relatively low superficial velocities. It takes a much longer time in terms of PV injected for gas to dissolve into unsaturated liquid (thus delaying the decline in pressure gradient [21]).

At higher superficial velocities and pressure gradients, liquid is forced across the entire core cross section, not just through a finger [21]. Moreover, the time for dissolution mass transfer is reduced relative to convection. Together these factors slow the formation and propagation of liquid fingers in terms of PV injected. Although the model is simplified, it can provide insights into the effect of shear-thinning behavior on the liquid injectivity in a SAG process.

As shown in Figs. 4 and 5, the propagation velocities and the total mobilities of the gas-dissolution bank and the forced-imbibition bank follow power-law relationships with the superficial velocities. The relationships are extrapolated to 2000 ft/day superficial velocity, in order to show the dimensionless velocities and total mobilities at an extremely high superficial velocity (at the injection well).

The parameter values of the power-law relationship shown in Eqs. (5)–(11) are fitted and listed as follows: $A = 4 \times 10^{-11}$, $B = 0.29$, $C = 0.1$, $D = -0.18$, $E = 5 \times 10^{-13}$, $F = 0.88$, $G = 2.7$, $H = -0.09$.

3.2. Radial flow

The banks propagate radially in the near-well region with the dimensionless velocities and total mobilities derived from the coreflood experiments. In the radial-flow model, we are interested in the pressure drop between the injection well and the outer radius (r_e), which we take to be 20 m. This corresponds to the equivalent radius around the injection well defined by Peaceman [22] for a 100 m × 100 m grid block. The wellbore radius (r_w) is 0.1 m. The porosity and the permeability are set as 0.2 and 160 mD, respectively, as in the linear-flow model. More details of the radial-flow model can be found in our previous work [20]. The grid-block pore volume (GPV) is defined as the pore volume of the grid block we assume in our calculation, i.e. block of 100 m × 100 m × 1 m dimensions. In all the cases examined, the dimensionless pressure drop is defined as the pressure difference between r_w and r_e normalized by the pressure difference caused by injecting water at the same volumetric rate

$Q_0 = 4.5 \times 10^{-4}$ m^3/s/m (39 m^3/d/m) into a fully water-saturated region. Since the dimensionless propagation velocities and the total mobilities of the banks during gas injection are not significantly affected by the gas superficial velocity, the estimated gas injectivity would be similar to that in our previous study [20]. Here we focus on illustrating the importance of considering the shear-thinning behavior on estimation of the liquid injectivity in a SAG process.

3.2.1. Radial-flow modelling with uniform bank properties

We first assume uniform bank properties as measured at different velocities in the separate experiments and show the effect on liquid injectivity. All the other modelling parameters are held fixed, including the injection rate Q_0. Injection rate Q_0 is set in the different cases such that, the superficial velocities from the well to the outer radius varies between about 200 ft/day and 1 ft/day. We adopt the bank properties as a function of radial position shown above.

Fig. 6 shows that the estimated liquid injectivity is significantly affected by the bank properties assigned. For liquid injection directly following foam (Fig. 6a), the maximum dimensionless pressure drop calculated using bank properties corresponding to 2 ft/day superficial velocity is about 180, while it is only about 5 with bank properties corresponding to 200 ft/day superficial velocity. For liquid injection following 10 GPV gas injection (Fig. 6b), a collapsed-foam bank forms near the injection well during the previous gas-injection period, which makes the dimensionless pressure drop lower than with liquid injection directly following foam. However, the peak dimensionless pressure drop estimated with bank properties at 2 ft/day superficial velocity is still about 20 times that estimated with bank properties at 200 ft/day superficial velocity. Intermediate-size gas slugs would of course produce effects between these two extremes.

Fig. 7 shows the effect of the size of the previous gas slug on the subsequent liquid injectivity. For all the liquid-bank properties examined, the more gas injected, the better subsequent liquid injectivity. Specially, the larger gas slug injected, the lower, longer-lasting plateau in pressure drop during subsequent liquid injection. After liquid penetrates the collapsed-foam bank and the forced-imbibition bank reaches the outer radius r_e, the plateau starts. The unsaturated injected liquid contacts virtually all gas in the collapsed-foam bank, delaying the formation of fingers [21]. Dissolution of gas delays arrival of unsaturated liquid at the forced-imbibition bank. The larger the gas slug injected, the larger the collapsed-foam bank, and the longer the plateau in

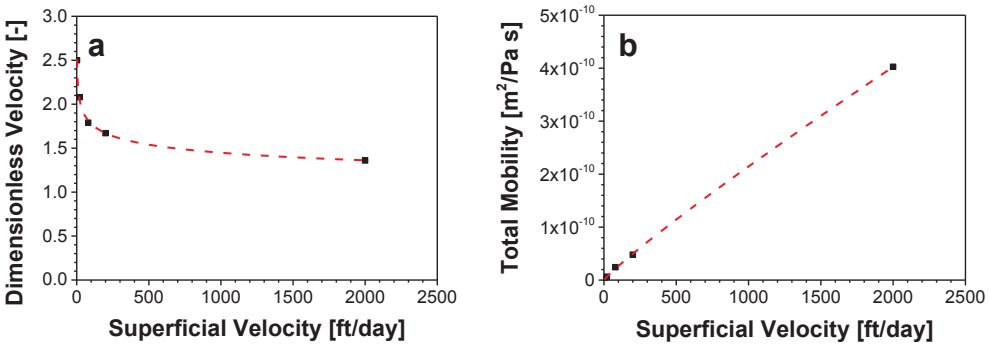

Fig. 4. Bank properties of the forced-imbibition bank during the liquid-injection period in a SAG process. (a) Dimensionless propagation velocity. (b) Total mobility.

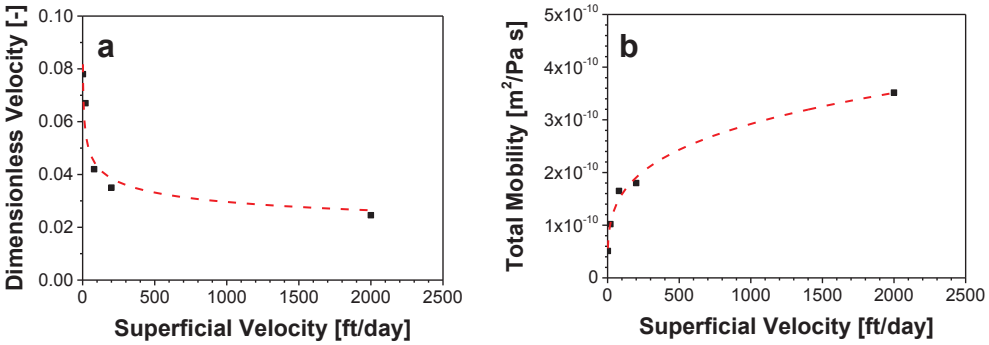

Fig. 5. Bank properties of the gas-dissolution bank during the liquid-injection period in a SAG process. (a) Dimensionless propagation velocity. (b) Total mobility.

pressure drop during liquid injection.

Comparing the dimensionless pressure drop calculated with bank properties corresponding to 2 ft/day and 200 ft/day, the difference between the two cases becomes smaller as more gas is injected, i.e. about 40 times for liquid injection following foam, while about 20 times for liquid injection following 30 GPV gas injection (Fig. 7).

Fig. 8 shows the effect of injection rate on liquid injectivity for liquid injection directly following foam and following 10 GPV gas injection. The constant dimensionless propagation velocity and the uniform total mobility correspond to the superficial velocity at the well for different injection rates are assumed within each bank. For example, for liquid injection at $Q_o = 4.5 \times 10^{-4}$ m^3/s/m, we assume uniform bank properties corresponding to 200 ft/day superficial velocity (the superficial velocity at the well). For liquid injection at $(1/100)Q_o$, we then assume uniform bank properties corresponding to 2 ft/day superficial velocity.

The results in Fig. 8 show strongly shear-thinning behavior. For liquid injection directly following foam, the peak dimensionless pressure drop is about 5 for liquid injection at Q_o, while it is about 1.8 for $0.01Q_o$. The maximum dimensionless pressure drop is only about 2.5 times higher, reflecting the extremely shear-thinning behavior in the forced-imbibition bank (Eq. (7)). At long times, the dimensionless pressure drop is about 25 times greater for the injection rate 100 times greater (Fig. 8a). This reflects the less-shear-thinning behavior in the gas-dissolution bank (Eq. (5)). Similar shear-thinning behavior is observed for the case of liquid injection after 10 PV gas injection, although the dimensionless pressure drop is lower than that for liquid injection directly following foam (Fig. 8b).

3.2.2. Radial-flow model with velocity-dependent bank properties

In this section, we examine the effect of velocity-dependent bank properties on liquid injectivity. Instead of assuming constant dimensionless propagation velocity and uniform total mobility within each bank, we include superficial-velocity-dependent properties for the forced-imbibition bank and the gas-dissolution bank (Eqs. (5)–(8)). For liquid flow in the collapsed-foam bank and the foam bank further away, we still assume uniform bank properties, since our laboratory results show that they are not significantly affected by the superficial velocity. Details can be found in Table 1.

Fig. 9 shows the effect of injection rate on liquid injectivity assuming velocity-dependent bank properties. For various injection rates, different ranges of superficial velocities from the well to the outer radius apply. For example, at injection rate $Q_o = 4.5 \times 10^{-4}$ m^3/s/m, the superficial velocities vary from 200 ft/day at the well to about 1 ft/day at the outer radius. For liquid injection at $(1/100)Q_o$, the superficial velocities vary from 2 ft/day at the well, to about 0.01 ft/day at the outer radius.

As shown in Fig. 9a, for liquid injection directly following foam at injection rate $10Q_o$, the peak dimensionless pressure drop is about 210, while it is about 80 for $0.01Q_o$. The pressure rise is about 2.5 times greater for an injection rate is 1000 times greater. It reflects the strongly shear-thinning behavior in the forced-imbibition bank (Eq. (7)). For liquid injection after 10 GPV gas injection

(Fig. 9b), the initial rise in injection pressure during liquid injection is about 2.8 times greater. The strongly shear-thinning behavior again reflects the forced-imbibition bank; the collapsed-foam bank does not contribute significantly to injection pressure.

Fig. 10 compares the liquid injectivity assuming velocity-dependent bank properties and assuming uniform bank properties corresponding to various superficial velocities. In this scenario, the injection rate is set at Q_o, so superficial velocity varies from 200 ft/day at the well to 1 ft/day at the outer radius. Fig. 10 shows liquid injectivity in various cases, including liquid injection directly following foam (Fig. 10a) and following different amounts of gas injection (Fig. 10b - d).

For liquid injection directly following foam (Fig. 10a), the peak dimensionless pressure drop allowing for velocity-dependent bank

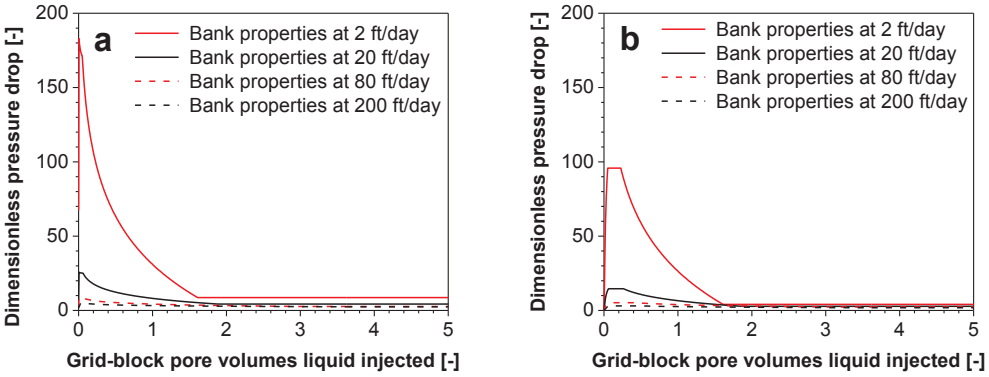

Fig. 6. Effect of bank properties corresponding to various superficial velocities on liquid injectivity. (a) Liquid injection directly following foam, (b) Liquid injection following 10 GPV gas injection.

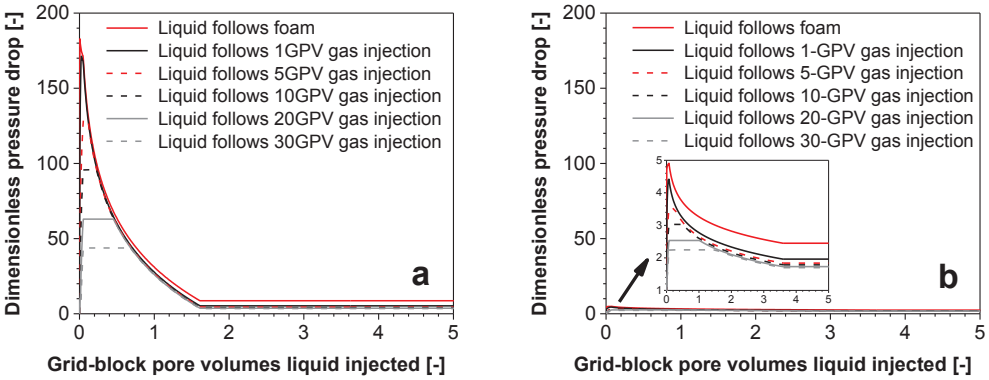

Fig. 7. Effect of gas-injection period on subsequent liquid injectivity. (a) Bank properties corresponding to 2 ft/day liquid superficial velocity. (b) Bank properties corresponding to 200 ft/day liquid superficial velocity.

properties is about 180. It is about 5 adopting the uniform bank properties at 200 ft/day; assuming these uniform bank properties overestimates liquid injectivity by about 30 times. Applying the uniform bank properties corresponding to a superficial velocity close to that at the outer radius

(2 ft/day) under- or overestimates the liquid injectivity at different times, but generally provides a better estimate of liquid injectivity than the other cases. Similar descriptions apply to the cases of liquid injection following a period of gas injection (Fig. 10b - d). Regardless of the amount of gas injection before the liquid slug, the dimensionless pressure drop calculated by assuming uniform bank properties comes closest to that with velocity-dependent properties if the uniform bank properties are close to those at the outer radius.

In conclusion, assuming uniform bank properties corresponding to the superficial velocity at the well can overestimate the liquid injectivity greatly. If one must assign uniform bank properties, properties close to those at the outer radius can provide a relatively reasonable estimation of the liquid injectivity, although there are still deviations.

3.3. Conventional simulation based on Peaceman equation

For comparison with the solution of the radial-bank-propagation model we calculate the dimensionless pressure drop as it would be represented in a conventional simulation based on the Peaceman equation. The foam model considered here is an “implicit texture” (IT) model [18], which represents the effect of foam on gas mobility through a mobility-reduction factor. The modelling approaches and assumptions are similar to our previous study [20]. Here we introduce the model only briefly, more details can be found in our previous work [20]. We focus on injectivity estimated for a 100 m × 100 m × 1 m grid block.

Table 1
Dimensionless propagation velocities and mobilities of the banks in a SAG process.

Period	Bank	Dimensionless velocity [–]	Total mobility [m^2/Pa s]
Gas injection	Collapsed-foam Bank	1.80×10^{-3}	3.52×10^{-9}
Gas injection	Foam Bank	Initially present*	2.34×10^{-11}
Gas injection	Water	Initially present*	1.50×10^{-10}
Liquid injection	Liquid slug in Collapsed-foam Bank	0.76	1.46×10^{-10}
Liquid injection	Forced-imbibition Bank	Eq. (8)	Eq. (7)
Liquid injection	Gas-dissolution Bank	Eq. (6)	Eq. (5)
Liquid injection	Foam Bank	Initially present	2.34×10^{-11}

* In the core-floods the initial state of the core is foam. In the radial-flow model, we assume initially the formation is saturated with liquid with $S_w = 1$. Foam advances in this case with a dimensionless velocity of 1.

The Peaceman equation [22] determines injectivity in most foam simulators. The water saturation in the grid block as a function of time is governed by a material balance on the grid block containing the injection well. We then apply the Peaceman equation to calculate the pressure rise at injection well during liquid injection in a SAG process [20]. The pressure drop between the injection well and the grid block containing the injection well is made dimensionless by dividing by the pressure drop of water injection into a fully water saturated reservoir at Q_o, as calculated using the radial-bank-propagation model.

The foam parameters are obtained by fitting the experimental data for a foam-quality (gas-fractional flow) scan at a fixed superficial velocity [20]. For a SAG foam process, the high-quality regime is more

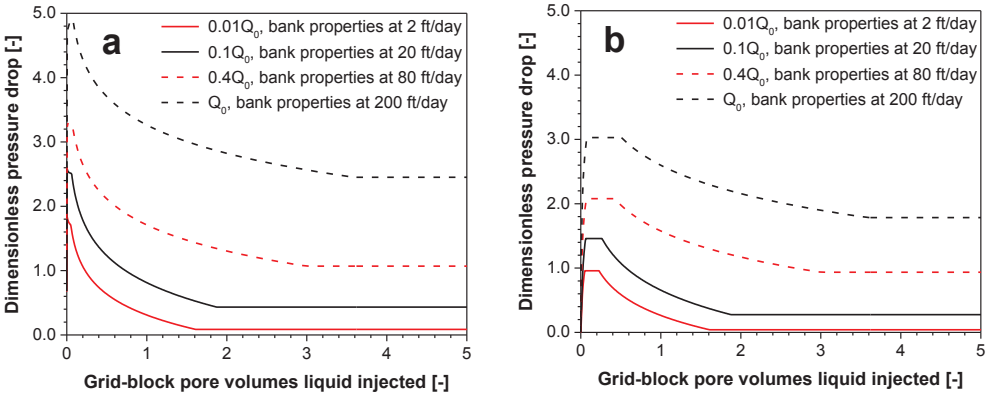

Fig. 8. Effect of injection rate on liquid injectivity. Bank properties correspond to the superficial velocity at well for different injection rates. (a) Liquid injection directly following foam. (b) Liquid injection following 10 GPV gas injection.

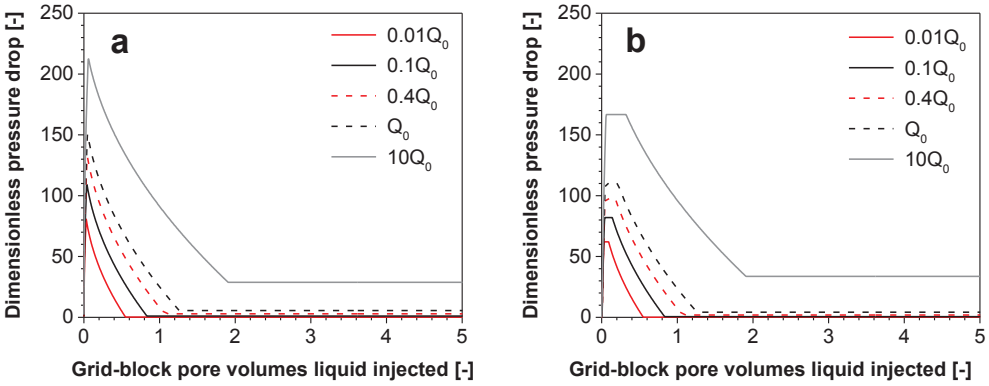

Fig. 9. Effect of injection rate on injection pressure during liquid injection. Bank properties depend on local superficial velocity. (a) Liquid injection directly following foam. (b) Liquid injection following 10 GPV gas injection.

relevant to the period of gas injection [23]. Thus, we neglect the foam parameters representing non-Newtonian behavior in the low-quality regime. We consider only the dry-out function, which is the dominant mechanism in the high-quality regime [18]. The details of parameter-fitting are described in our previous work [20].

The following assumptions are made for the calculations based on the Peaceman equation: 1. We assume foam immediately reaches local equilibrium. 2. Water saturation in the grid block is uniform at all times. 3. The effect of gravity is not considered. 4. Water, gas and rock are assumed to be incompressible. 5. Oil is not present in the region of interest. 6. Fingering is not considered.

In our previous study [20], we showed that a conventional foam simulator based on the Peaceman equation underestimates gas and liquid injectivities. Moreover, the conventional foam simulator cannot represent the effect of gas injection on the subsequent liquid injectivity in a SAG process without exceptional grid refinement near the well. Our experimental results suggest that the gas-injection period is not significantly affected by gas superficial velocity. Here we focus on the implication of the shear-thinning behavior during the liquid-injection period on field application.

As presented in Fig. 11, the dimensionless pressure drop during liquid injection estimated with the Peaceman equation increases proportionally to injection rate.

Fig. 12 shows that the liquid injectivity estimated by the conventional foam simulator is not affected by the amount of gas injected previously. The water saturation in the grid block is virtually unaffected by liquid injection rate, or the amount of gas injected previously (Fig. 12b).

Fig. 13 compares the liquid injectivity estimated by the conventional foam simulator using the Peaceman equation and our bank-propagation model with velocity-dependent bank properties. At a low injection rate ($0.01Q_o$), the Peaceman equation overestimates the

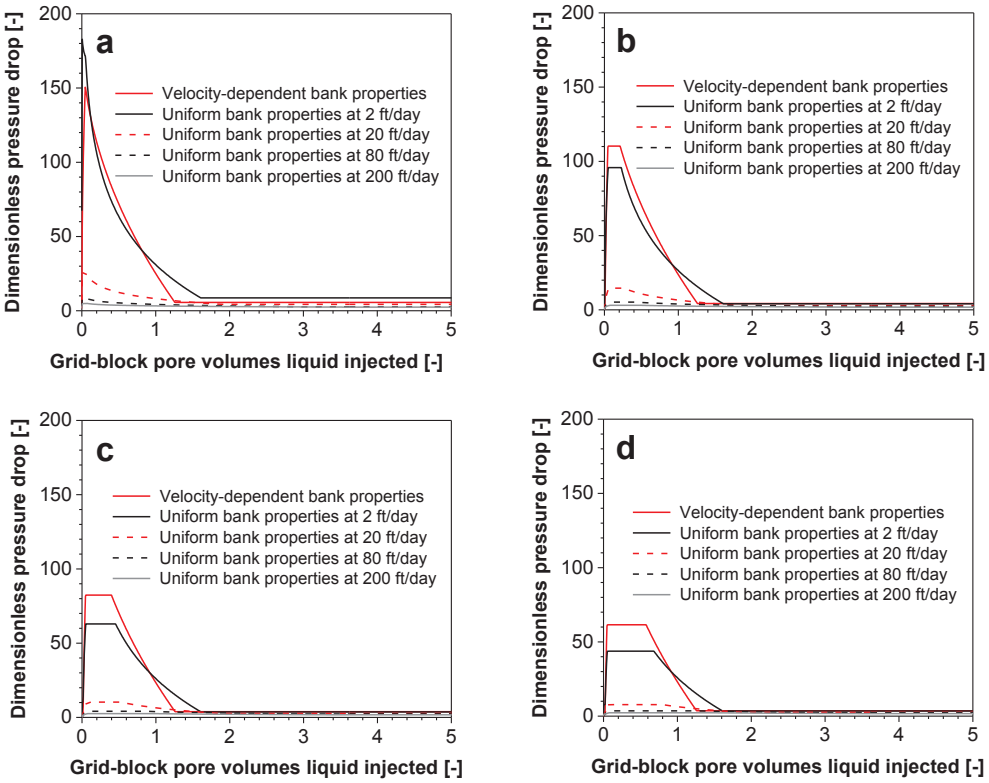

Fig. 10. Effect of non-uniform bank properties on liquid injectivity. (a) Liquid injection following foam. (b) Liquid injection following 10 GPV gas injection. (c) Liquid injection following 20 GPV gas injection. (d) Liquid injection following 30 GPV gas injection.

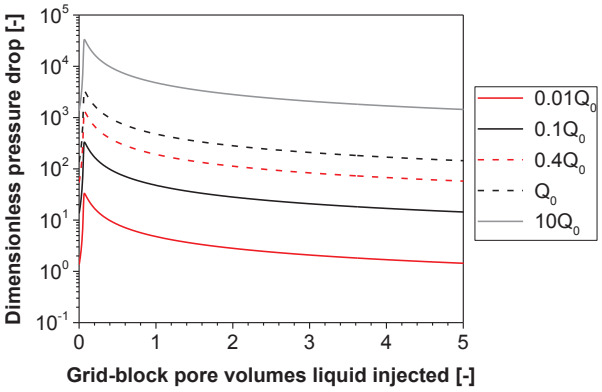

Fig. 11. Dimensionless pressure drop during liquid injection after 10 PV gas injection calculated from Peaceman equation. Liquid is injected at various injection rates ranging from $0.01Q_o$ to $10Q_o$.

minimum liquid injectivity by about 2 times, but it underestimates liquid injectivity at later times by about 25 times. At a high injection rate ($10Q_o$), the Peaceman equation underestimates the minimum liquid injectivity at first by more than 100 times, and later by about 40 times. The Peaceman equation does not provide a reliable prediction of the liquid injectivity in a SAG process, at least in a relatively large grid block.

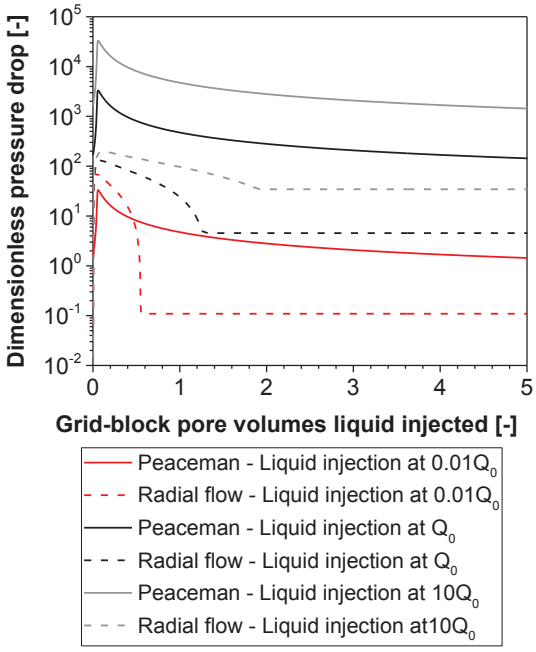

Fig. 13. Comparison of liquid injectivity following 5 PV gas injection calculated with Peaceman equation and the bank-propagation model with velocity-dependent bank properties.

4. Discussion

We estimate dimensionless propagation velocities and total mobilities of various banks at various superficial velocities from our laboratory data [21].

For the gas injection period, we examine three superficial velocities: 3 ft/day, 6 ft/day and 9 ft/day. These velocities tested the limits of our apparatus. Within this limit range, there was no significant variation of propagation velocities or mobilities with superficial velocity. In this study, our focus is on the liquid injectivity in a SAG process. This limitation would not significantly change the bank propagation velocities or total mobilities for the liquid-injection period.

For the liquid-injection period, our bank-propagation model can fit the experimental results well for liquid injection at relatively low superficial velocities, but captures the details at high superficial velocities less well. Nonetheless, it provides reasonable fit.

The power-law relationships of the dimensionless propagation velocity and total mobility with superficial velocity for the forced-imbibition and gas-dissolution banks are derived from one set of experiments conducted in one core sample. It may not be apply to other situations. Specifically, our experimental results, and in turn our modeling, depends on porous medium, surfactant, type of gas, pressure, temperature and other factors. A new set of experiments should be conducted for each different application.

The model we introduced is based directly on experimental data, but contains many assumptions. One major assumption is that the core-scale behavior scales up to field application. The effects of foam collapse during gas injection and of liquid fingering and gas dissolution during liquid injection are difficult to extrapolate from core scale to field scale.

The model is not predictive. Some deviations between the model and the data remain. However, it does show clearly that conventional foam simulators based on the Peaceman equation can greatly underestimate liquid injectivity in a SAG process. Crucial mechanisms are missing from the simulators, such as liquid fingering through gas, gas dissolution in unsaturated liquid, shear-thinning behavior during the liquid-injection period and the effect of previous gas injection on subsequent liquid injectivity. Grid resolution is also important with slow-moving banks like that for foam collapse during gas injection.

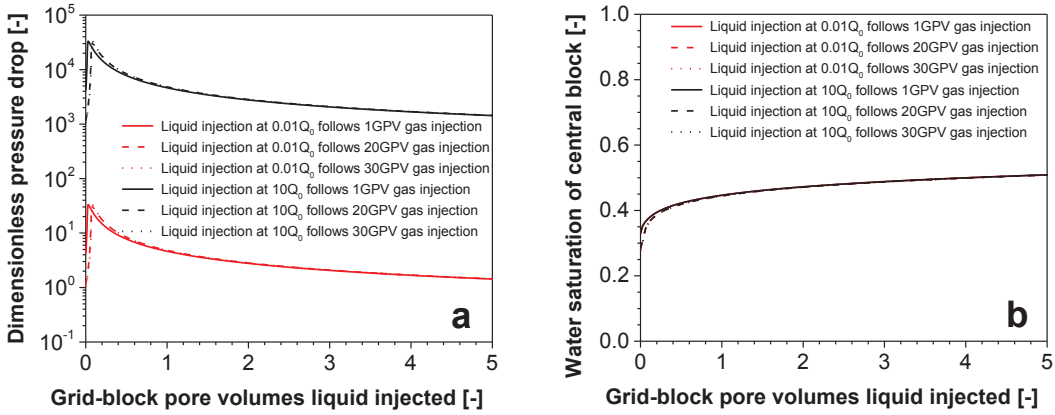

Fig. 12. Liquid injection at different rates following different amounts of gas injection. (a) Dimensionless pressure drop. (b) Water saturation of block containing injection well.

5. Conclusions

In this study, we investigate the implication of the strongly shear-thinning behavior of the gas-dissolution bank and forced-imbibition bank during the liquid-injection period observed in coreflood experiments on field application.

- Our simplified bank-propagation model gives reasonable fit to our experimental data, though some deviations between the model and the laboratory data remain.
- The velocity-dependent total mobilities and propagation velocities of the gas-dissolution bank and the forced-imbibition bank have major impact on the estimation of the liquid injectivity in a SAG process.
- Liquid injectivity is strongly affected by the liquid injection rate due to the shear-thinning behavior during the liquid-injection period. This should be considered in estimation of the liquid injectivity in a SAG process.
- If one must use fixed parameters based one superficial velocity of liquid, the best choice is to use the ones close to those apply at the outer radius.
- Conventional foam models based on the Peaceman equation do not represent the effect of a period of gas injection on the subsequent liquid injectivity, the propagation of various banks, or the shear-thinning behavior during liquid injection in a SAG process.
- Our modelling indicates that the conventional foam models can underestimate or overestimate the liquid injectivity, depending on the liquid injection rate. The greater the injection rate, the greater the error in conventional models.
- Due to the shear-thinning behavior, reducing liquid injection rate would not reduce the pressure at injection well proportionally to injection rate.

CRediT authorship contribution statement

Jiakun Gong: Conceptualization, Software, Writing - original draft. **Wendy Flores Martinez:** Investigation. **Sebastien Vincent-Bonnieu:** Conceptualization, Formal analysis. **Ridhwan Zhafri Kamarul Bahrim:** Validation, Resources. **Che A Nasser Bakri Che Mamat:** Resources, Project administration. **Raj Deo Tewari:** Resources, Project administration. **Mohammad Iqbal Mahamad Amir:** Validation. **Rouhollah Farajzadeh:** Conceptualization, Formal analysis. **William Rossen:** Conceptualization, Writing - review & editing, Supervision.

Declaration of Competing Interest

The authors declare that they have no known competing financial interests or personal relationships that could have appeared to influence the work reported in this paper.

Acknowledgement

We gratefully thank PETRONAS and Shell Global Solution International B.V. for supporting this work. We also thank the technical support of Michiel Slob at the Laboratory Geoscience and Engineering of Delft University of Technology.

References

[1] Lake LW, Johns RT, Rossen WR, Pope G. Fundamentals of Enhanced Oil Recovery. Richardson: Texas, USA, Society of Petroleum Engineers; 2014.
[2] Schramm LL. Foams Fundamentals and Applications in the Petroleum Industry. Advances in Chemistry Series. 242. Washington, DC: American Chemical Society; 1994.
[3] Kovscek AR, Radke CJ. Fundamentals of Foam Transport in Porous Media. Foams: Fundamentals and Applications in the Petroleum Industry. Advances in Chemistry, American Chemical Society; 1994. p. 115–63. Chap. 3.
[4] Rossen WR. Foams in enhanced oil recovery. In: Prud'homme RK, Khan SA, editors. Foams: Theory, Measurements and Applications. New York City: Marcel Dekker; 1996. p. 413–64.
[5] Matthews CS. Carbon dioxide flooding. In: Donaldson EC, Chilingarian GV, Yen TF, editors. Developments in Petroleum Science. Amsterdam: Elsevier; 1989. p. 129–56.
[6] Heller JP. CO2 Foams in Enhanced Oil Recovery. Foams: Fundamentals and Applications in the Petroleum Industry. Advances in Chemistry, American Chemical Society; 1994. p. 201–34. Chap. 5.
[7] Kibodeaux KR, Rossen WR. Coreflood study of surfactant-alternating-gas foam processes: implications for field design. SPE Western Regional Meeting, Long Beach, California, USA 1997. https://doi.org/10.2118/38318-MS.
[8] Shan D, Rossen WR. Optimal injection strategies for foam IOR. SPE J 2004;9(02):132–50.
[9] Rossen WR, van Duijn CJ, Nguyen QP, Shen C, Vikingstad AK. Injection strategies to overcome gravity segregation in simultaneous gas and water injection into homogeneous reservoirs. SPE J 2010;15(01):76–90. https://doi.org/10.2118/99794-PA.
[10] Le VQ, Nguyen QP, Sanders AW. A novel foam concept with CO_2 dissolved surfactants. SPE/DOE Symposium on Improved Oil Recovery, Tulsa, OK, USA. 2008.
[11] Xing D, Wei B, McLendon W, Enick RM, McNulty S, Trickett K, et al. CO2-soluble, nonionic, water-soluble surfactants that stabilize CO_2-in-brine foams. SPE J 2012;17(04):1172–85.
[12] Kuehne DL, Ehman DI, Emanuel AS, Magnani CF. Design and evaluation of a nitrogen-foam field trial. J Petrol Technol 1990;42(02):504–12.
[13] Martinsen HA, Vassenden F. Foam-assisted water alternating gas (FAWAG) process on Snorre. European IOR Symposium, Brighton, UK 1999. https://doi.org/10.3997/2214-4609.201406335.
[14] Gong J, Vincent Bonnieu S, Kamarul Bahrim RZ, Che Mamat CANB, Groenenboom J, Farajzadeh R, et al. Laboratory investigation of liquid injectivity in surfactant-alternating-gas foam enhanced oil recovery. Transp Porous Med 2020;131:85–99.
[15] Persoff P, Radke CJ, Pruess K, Benson SM, Witherspoon PA. A laboratory investigation of foam flow in sandstone at elevated pressure. SPE Reservoir Eng 1991;6(03):365–71.
[16] Kibodeaux KR, Zeilinger SC, Rossen WR. Sensitivity study of foam diversion processes for matrix acidization. SPE Annual Technical Conference and Exhibition, New Orleans, Louisiana, USA 1994. https://doi.org/10.2118/28550-MS.
[17] Zeilinger SC, Wang M, Kibodeaux KR, Rossen WR. Improved Prediction of Foam Diversion in Matrix Acidization. SPE Production Operations Symposium, Oklahoma City, Oklahoma, USA. 1995.
[18] Cheng L, Reme AB, Shan D, Coombe DA, Rossen WR. Simulating Foam Processes at High and Low Foam Qualities. SPE/DOE Improved Oil Recovery Symposium, Tulsa, Oklahoma. 2000.
[19] Nguyen QP, Zitha PLJ, Currie PK, Rossen WR. CT Study of liquid diversion with foam. SPE Prod Oper 2009;24(01):12–21.
[20] Gong J, Vincent Bonnieu S, Kamarul Bahrim RZ, Che Mamat CANB, Groenenboom J, Farajzadeh R, et al. Modelling of liquid injectivity in surfactant-alternating-gas foam enhanced oil recovery. SPE J 2019;24(3):1123–38. SPE-190435-PA.
[21] Gong J, Flores Martinez W, Vincent Bonnieu S, Kamarul Bahrim RZ, Che Mamat CANB, Farajzadeh R, et al. Effect of superficial velocity on liquid injectivity in SAG Foam EOR. Part 1: experimental study. Fuel 2020. [Accepted].
[22] Peaceman DW. Interpretation of well-block pressures in numerical reservoir simulation. SPE J 1978;18(03):183–94.
[23] Rossen WR, Boeije CS. Fitting foam-simulation-model parameters to data: II. surfactant-alternating-gas foam applications. SPE Reservoir Eval Eng 2015;18(02):273–83.